Mike Daily*
Radar Remote Sensing Team
Jet Propulsion Laboratory
Pasadena, CA 91103

Hue-Saturation-Intensity Split-Spectrum Processing of Seasat Radar Imagery

Filtering a scene into low-frequency and high-frequency components, then assigning hue and intensity, respectively, provides a considerable improvement in the detectability of subtle geological structures.

Abstract: *Seasat radar images of terrain can be modeled as a superposition of (1) low-frequency tone variations associated with vegetation and lithologic contrasts, and (2) heavily modulated high-frequency features representing sloping targets facing the radar. Filtering the scene into low-frequency and high-frequency components, then assigning hue and intensity, respectively, provides a considerable improvement in the detectability of subtle geological structures at all scales. This technique was applied to a test site in southwestern Wyoming characterized by a monotonous Tertiary clastic section and gentle folds. Major structural features, invisible on the original Seasat radar image, are clearly displayed on the enhanced version.*

Introduction

The Seasat synthetic-aperture radar (SAR) has been used in a variety of geologic and oceanographic applications (Elachi, 1980). Study areas have included heavily vegetated mountainous terrain (Ford, 1980) and arid sand seas (Blom and Elachi, 1981). These studies have demonstrated the importance of reflections from small slopes facing toward the radar. In the Appalachian Mountains, these bright slopes aided in the identification of lineaments, although they introduced a considerable directional bias (Ford, 1980). For dune fields, specular (mirror-like) reflections from metre-scale facets were the dominant sources of return echo (Blom and Elachi, 1981).

Reflection from slopes can be a problem, however, in certain terrain. The large sedimentary basins of Tertiary age in Wyoming and adjacent states are characterized by a rather monotonous clastic section and gentle fold structures. Vegetation cover is sparse to moderate, and relief is typically low to moderate. One of the most important applications of orbital radar imagery in such terrain is the mapping of large fold structures whose subtle expression on radar images results from slight variations in vegetation density or surface roughness.

In practice, detection of these large subtle features is very difficult because of the distracting effect of small bright features that result from reflection from gullies and other small-scale topography. The following sections provide physical explanations for this effect in terms of radar imaging physics and the characteristics of the human visual system. Based on this physical insight, we describe an image-enhancement technique that improves the display of subtle large-scale features while retaining fine detail.

* Now with the Mobil Research and Development Corporation, P.O. Box 900, Dallas, TX 75221.

Photogrammetric Engineering and Remote Sensing,
Vol. 49, No. 3, March 1983, pp. 349-355.

0099-1112/83/4903-0349$02.25/0

Radar Imaging Physics

Imaging radars have several properties that set them apart from typical optical sensors:

- Transmitter and receiver are colocated; retroreflection is therefore important.
- Variation in return is dominated by scattering rather than electrical properties.
- Radar is a ranging sensor; large non-linear distortions exist due to look angle and relief displacement (foreshortening) effects.

The combination of these properties is responsible for radar's extreme sensitivity to small-scale topography. The intensity of retroreflection from slopes oriented normal to the radar illumination depends upon the roughness and areal extent of the surface presented to the radar. True specular reflection implies a surface that is smooth at the scale of the radar wavelength and is many wavelengths in areal dimension. True specular targets, such as sand dunes, have very high reflectivity. Rougher slopes, such as forested hillslopes, have much lower reflectivity per unit area, but are commonly quite bright on the image due to foreshortening. In this paper, both specular and foreshortening effects are taken to be examples of a general slope effect.

For steep-incidence radars such as the Seasat SAR ($\theta \sim 20°$), the above properties are responsible for strong returns from targets oriented normal to the illumination vector (Figure 1). This reflection mechanism is important in radar mapping at regional scale because (1) returns are generally confined to the high spatial frequencies in a scene because 20° slopes are rare at scales greater than a few kilometres, and (2) slope-dominated returns are extremely powerful compared to other scattering mechanisms. The practical consequence of the slope effect in images of low to moderate-relief terrain is that subtle large-scale features such as lithologic or vegetation contrasts are masked by heavily modulated high-frequency tone variations associated with small drainages.

Spatial Frequency Content

The power spectrum of many radar images (shown schematically in Figure 2) contains three major components:

- A low-frequency component dominated by variations in surface scattering.
- Higher-frequency tone variations driven by slope effects, including specular returns.
- Underlying broadband noise, termed speckle.

Note that the curves for surface properties and topography in Figure 2 intersect at f_c, the crossover frequency. As a measure of the transition from diffuse to slope-dominated scattering, define

$$\Lambda_c = 1/f_c \text{ in kilometres}$$

Another measure of interest is the low-frequency, half-power (−3dB) point on the topography curve, f^*, from which define

$$\Lambda^* = 1/f^* \text{ in kilometres (Figure 3)}$$

Three general cases can be distinguished (Figure 4):

Case 1: $\Lambda_c > \Lambda^*$. This situation implies the presence of strong, high frequency slope-dominated returns imbedded in an otherwise monotonous scene. A good example of this is the limestone terrane of the Caribbean, where a forested plateau is riddled with small karst depressions.

Case 2: $\Lambda_c \approx \Lambda^*$. This is the most common situation in low-to-moderate relief terrain.

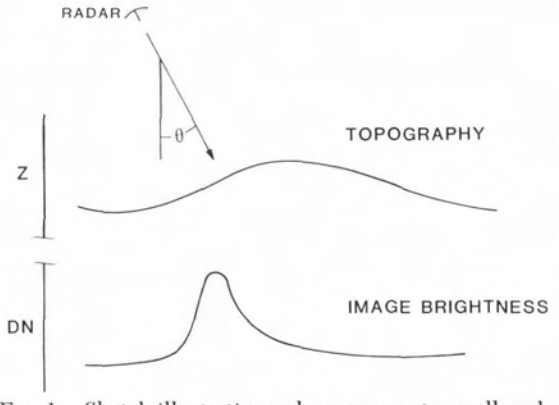

Fig. 1. Sketch illustrating radar response to small-scale topography. Image brightness is sharply peaked at normal incidence.

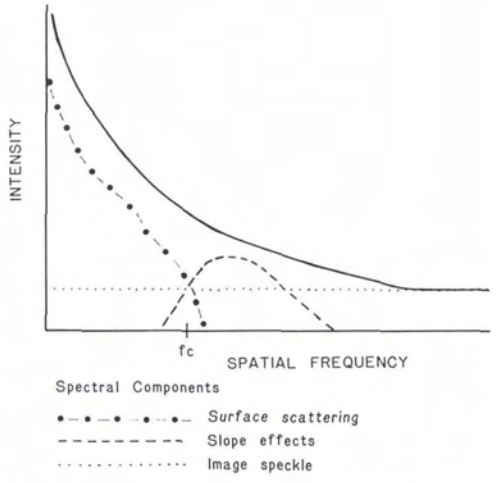

Fig. 2. Schematic power spectrum of radar image. Total spectrum has contributions from surface scattering, topographic effects, and speckle noise.

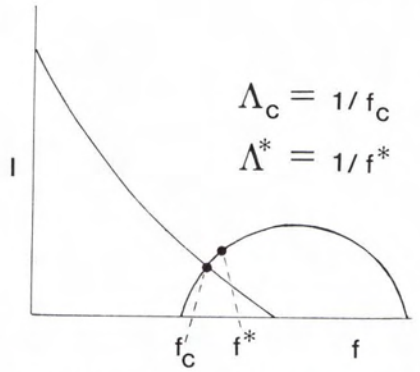

FIG. 3. Model power spectrum showing surface and topography curves. f_c and f^* are defined in text.

Case 3: $\Lambda_c < \Lambda^*$. Two types of terrain have this situation:

- Extremely flat areas such as coastal plains where diffuse scattering dominates the power spectrum at all frequencies.
- Extremely rough mountainous regions where slope-dominated returns from long steep slopes contribute energy to the low-frequency end of the spectrum.

This study concentrates on Case 2, because this situation (1) has significant low-frequency information content (in contrast to Case 1); and (2) has surface and topographic components that are separable by filtering (in contrast to Case 3).

Although a simple, low-pass filtering operation can provide some information on surface properties, a proper interpretation of a scene also requires the high-frequency visual cues associated with minor drainages. As an example, Figure 5 shows a Seasat radar image of an area near Patrick Draw, Wyoming. Also shown are low-frequency and high-frequency images derived by spatial filtering of the original scene.

Psychophysics of Human Vision

The spatial frequency response of the human visual system has been summarized by Pratt (1978). Figure 6 shows chromatic (hue) and achromatic (intensity) spatial frequency responses of the human visual system measured by van der Horst *et al.* (1967) and Davidson (1968), respectively. The maximum achromatic response occurs near 7 cycles/degree, rolling off substantially toward higher and lower frequencies. The low-frequency half-power (−3dB) point occurs near 2.5 cycles/degree and provides a convenient measure for the onset of serious information loss. In terms of spatial dimensions, the wavelengths of interest are given by

$$\lambda_{max} = X \tan\frac{1}{7} = X(0.0025) \qquad (1)$$

$$\lambda_{(-3dB)} = X \tan\frac{1}{2.5} = X(0.007) \qquad (2)$$

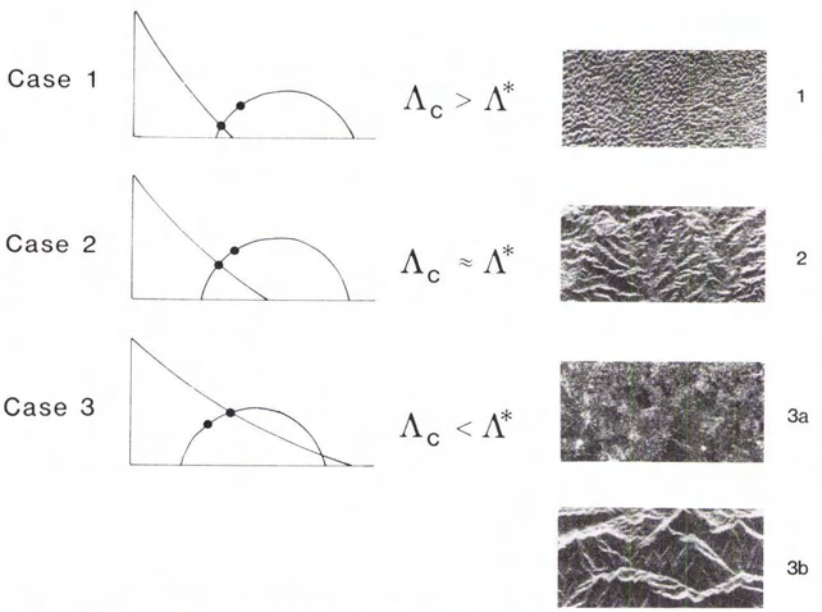

FIG. 4. Model spectra of radar images from several terrain types. Refer to Figure 3. Case 1 is limestone Karst terrane. Case 2 is moderately rough hilly terrain. Case 3a is a smooth coastal plain, while 3b is extremely rough, mountainous terrain.

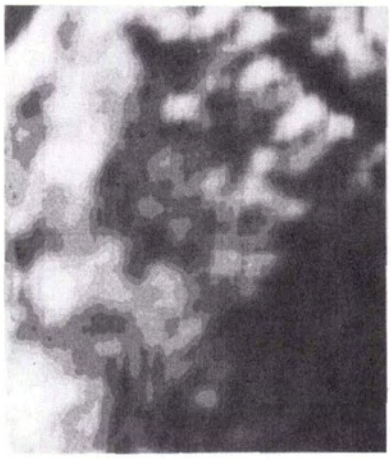

FIG. 5. Seasat radar image of Patrick Draw, Wyoming site. (a) Original scene, (b) low-pass filtered (F = 101), and (c) high-pass filtered (F = 101).

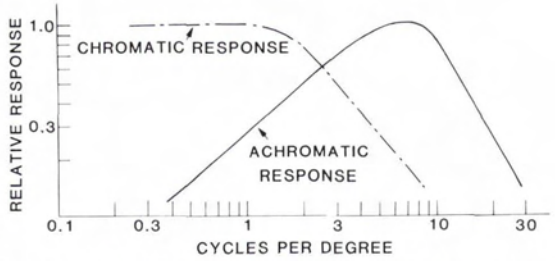

FIG. 6. Spatial frequency response of the human visual system (after Pratt, 1978).

where X is the spacing between eye and scene (Figure 7). Table 1 summarizes λ_{-3dB} for several such viewing distances and also tabulates values of λ^*, the ground scale (in kilometres) of features falling at the half-power point, for several image scales: i.e.,

$$\lambda^* = \lambda_{(-3dB)} \cdot S \cdot 10^{-5}$$

where (1:S) is the scale of the image.

As an example, a black-and-white (achromatic) picture of scale 1:500,000 viewed from one metre will have, from Equations 2 and 3,

$$\lambda^* = 3.5 \text{ km}$$

and, from 1,

$$\lambda_{max} = 0.25 \text{ cm}$$

which is equivalent to 1.25 km on the ground. Thus, features having dimensions of approximately one kilometre will be perceived with maximum acuity, whereas larger features (3.5 kilometres) will excite half that response in the human visual system.

The chromatic spatial frequency response of the human visual system strongly favors the low frequencies (Figure 6). Note that the response axis is relative; therefore, the fact that the crossing frequency and the half-power points are nearly coincident is of no fundamental significance. Presumably, the chromatic response could be equalized with the achromatic by adjusting color saturation or by changing the achromatic contrast ratio.

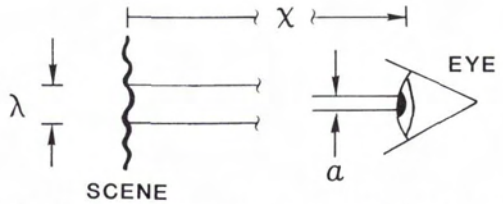

FIG. 7. Eye-scene geometry. Quantities defined in text.

TABLE 1. λ_{-3dB} AND λ^* FOR SEVERAL VIEWING DISTANCES

X (cm)	λ_{max} (cm)	λ_{-3dB} (cm)	λ^*(km) 1:48,000	1:125,000	1:500,000
25	0.06	0.17	0.08	0.21	0.85
50	0.12	0.35	0.17	0.44	1.8
75	0.19	0.52	0.25	0.65	2.6
100	0.25	0.70	0.34	0.87	3.5

HSI SPLIT SPECTRUM PROCESSING

The hue-saturation-intensity (HSI) transformation described in Appendix A provides a convenient mechanism for displaying two or three data sets independently on the same image. The HSI split-spectrum process exploits the spatial frequency properties of the radar image and the human visual system.
The process includes

- Estimation of Λ_c from field data, inspection of imagery, or use of elevation or slope data.
- Digital filtering using a filter size (F) of

$$F = \frac{\Lambda_c}{P}$$

where P is the pixel size in kilometres on the ground, to yield high-pass and low-pass images. Note that the kernel sizes for the filters could be adjusted to account for cases where $\Lambda_c \neq \Lambda^*$.

- Assignment of hue to the low-frequency scene and intensity to the high-frequency scene.
- Adjustment of color saturation and intensity contrast to balance response. This subjective process is best performed interactively.
- Conversion to RGB color space followed by playback onto film.
- Color printing to a scale that is optimized for human visual characteristics: i.e.,

$$S = \frac{\Lambda_c \cdot 10^5}{X \cdot 0.007}$$

where $(1{:}S)$ = Image scale

$$\Lambda_c = \frac{1}{f_c} \text{ (km), and}$$

X = eye-scene distance (cm).

For Seasat SAR digital images, $S = \Lambda_c \cdot 285{,}714$ for $X = 50$ cm, a common viewing distance.

PATRICK DRAW, WYOMING SITE

The primary geologic structure in this scene is the Wamsutter Arch, a plunging anticline. Although it is known from subsurface data, the Arch has not been located well by field techniques because of the paucity of marker beds in the Wasatch and Ft. Union formations. Note that none of the three images in Figure 5 offers a particularly clear indication of such a structure.

Field work in the area indicates that radar backscatter is dominated by number density of shrubs, primarily Artemisia tridentata (Big Sage brush) (Figure 8). The vegetation density is in turn influenced by soil type, topography, availability of nutrients and moisture, and perhaps subtle effects from leaking hydrocarbons and associated trace chemical species. Insofar as these influences are correlated with particular portions of the geologic column, plunging folds should be detectable on radar imagery. Unfortunately, these large subtle features tend to be suppressed by the two mechanisms described above, namely

- The extreme enhancement of high spatial frequencies by slope-dominated returns and, locally, by scattering from riparian vegetation.
- Low frequency roll-off of the spatial frequency response of the human visual system.

FIG. 8. Oblique ground photograph near Patrick Draw site showing sage and grass plant community. Scale bar in the foreground is 15 cm.

Application at Patrick Draw

For this 2000-pixel-square scene, F was chosen to be 101, corresponding to $\Lambda_c = 2.5$ km. The resulting color output (see cover) is an improvement over the original scene. The series of nested arcuate color zones transected by the black line represent outcrops folded by the Wamsutter Arch. The position of the structure is in good agreement with subsurface data and processed Thematic Mapper Simulator (TMS) data (Lang, personal communication). An arcuate drainage marked by D on the cover photo lies off the axis of the structure.

In addition to an improved display of low-frequency structural data, the split-spectrum picture also provides a better format for mapping lineaments. Inspection of a 1:4800 enlargement shows that many lineaments consist of two spatial frequency components:

- A sharp bright line that modulates intensity, and
- a broader brightness gradient that is expressed as a color variation.

Figure 9 shows schematically a brightness profile across one of the lineaments. The encoding of high and low frequencies as intensity and hue, respectively, improves the detectability of lineaments, especially at the large image scales used for photointerpretation.

Conclusions

The HSI split-spectrum process exploits the properties of radar sensor-target interaction and the spatial frequency response of the human visual system to restore low spatial frequencies to Seasat SAR imagery. The process provides separate encoding of surface scattering and topographic effects and has resulted in the detection of a large plunging anticline in Wyoming from an orbital platform.

Acknowledgments

James Soha and Susan Williams of the Image Processing Laboratory at JPL provided assistance in the interactive processing. Harold Lang, Ron Blom, and John McKeon (Gulf Oil) provided comments on the Patrick Draw site. This paper represents one phase of research carried out at the Jet Propulsion Laboratory under Contract NAS7-100.

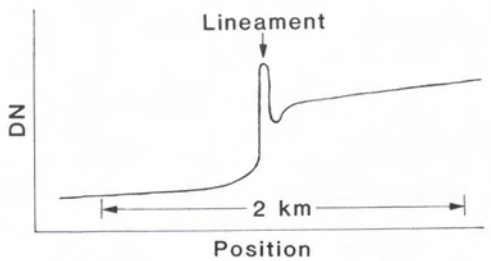

Fig. 9. Brightness profile (schematic) across a lineament on the Seasat radar image illustrating high and low frequency components.

References

Blom, R., and C. Elachi, 1981. Spaceborne, and Airborne Imaging Radar Observations of Sand Dunes, *Jour. Geophys. Res.*, 86, pp. 3061-3073

Davidson, M. L., 1968. Perturbation Approach to Spatial Brightness Interaction in Human Vision, *J. Opt. Soc. Am.*, 58, pp. 1300-1308.

Elachi, C., 1980. Spaceborne Imaging Radar: Geologic and Oceanographic Applications, *Science*, 109, pp. 1073-1082.

Ford, J. P., 1980. Seasat Orbital Radar Imagery for Geologic Mapping, Tennessee-Kentucky-Virginia, *AAPG Bull.*, 64, pp. 2064-2094.

Gillespie, A. R., 1980. Digital Techniques of Image Enhancement, in B. S. Siegal and A. R. Gillespie, *Remote Sensing in Geology*, John Wiley, p. 702.

Pratt, W. K., 1978. *Digital Image Processing*, John Wiley, 750 p.

Van der Horst, C., C. M. de Weert, and M. A. Bouman, 1967. Transfer of Spatial Chromaticity-Contrast at Threshold in the Human Eye, *J. Opt. Soc. Am.*, 57, pp. 1260-1266.

(Received 21 August 1981; revised and accepted 8 December 1982)

Appendix A
The HSI Color Coordinate System (after Gillespie, 1980)

The hue-saturation-intensity color coordinate system describes color in terms of three independent physiological parameters. Hue is a measure

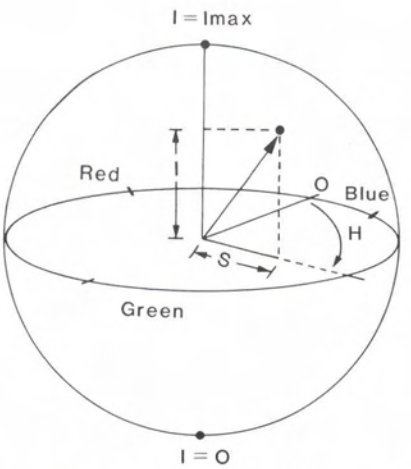

Fig. A-1. Hue (H)-Saturation (S)-Intensity (I) color coordinate system.

of the average wavelength of light reflected by an object. Saturation is a measure of the spread of colors, ranging from pure saturated color through less saturated pastel to unsaturated gray. Intensity is a measure of total reflectance in the visible region and is, therefore, the achromatic component of perceived color.

These relations are commonly represented in a spherical coordinate system where H (hue) is longitude, S (saturation) is colatitude, and I (intensity) is radius (Figure A-1). For the purposes of this study, the perceived independence of hue and intensity is used to separate low from high spatial frequencies in a radar image. A transformation is then applied consisting of a spherical-to-rectangular coordinate conversion followed by coordinate rotation. This transformation maps HSI into RGB (red-green-blue) color space for display.

In this study, $H = 0$ was defined as blue and $H = 255$ as red. This maintains a simple spectral progression without duplication of colors. Saturation and contrast (local range of intensity) were varied interactively to equalize apparent response to the chromatic and achromatic features.

39th Photogrammetric Week

Stuttgart, Federal Republic of Germany
19-24 September 1983

The 39th Photogrammetric Week is sponsored by the Institute for Photogrammetry of Stuttgart University and the Division for Surveying and Photogrammetry of Carl Zeiss, Oberkochen. This regular event was initiated by Carl Pulfrich as a "vacation course in Photogrammetry" in 1909. This is its sixth time in Stuttgart since 1973.

As in previous years, Prof. F. Ackermann, Stuttgart, and Prof. H.-K. Meier, Oberkochen, are responsible for the scientific direction. The lecturers, from Germany and abroad, will put special emphasis on

- Data processing with analytical systems
- Orthophotography
- Digital image processing for photogrammetric purposes

Experienced technical interpreters will give simultaneous translations of the mostly German lectures into English, French, and Spanish. The lectures will be unabridged; sufficient time has been allowed for discussions. The program will include demonstrations and practical exercises on three afternoons.

For further information please contact

Institut für Photogrammetrie
Universität Stuttgart
Postfach 560
Keplerstrasse 11
D-7000 Stuttgart 1
Federal Republic of Germany